



Contents lists available at ScienceDirect

Computers and Structures

journal homepage: [www.elsevier.com/locate/compstruc](http://www.elsevier.com/locate/compstruc)

# Numerical determination of concrete crack width for corrosion-affected concrete structures

S.T. Yang<sup>a,\*</sup>, K.F. Li<sup>b</sup>, C.Q. Li<sup>c</sup><sup>a</sup> Department of Civil and Environmental Engineering, University of Strathclyde, Glasgow G1 1XJ, United Kingdom<sup>b</sup> Department of Civil Engineering, Tsinghua University, Beijing 100084, China<sup>c</sup> School of Engineering, RMIT University, Melbourne, VIC 3000, Australia

## ARTICLE INFO

### Article history:

Accepted 26 July 2017

Available online xxxxx

### Keywords:

Corrosion

Crack width

Reinforced concrete

Numerical modelling

## ABSTRACT

Corrosion-induced deterioration of reinforced concrete (RC) structures results in premature failure of the RC structures. In practice concrete crack width is one of the most important criteria for the assessment of the serviceability of RC structures. It is therefore desirable to predict the growth of the crack width over time so that better informed decisions can be made concerning the repairs due to concrete cracking. Literature review shows that little research has been undertaken on numerical prediction of concrete crack width. The intention of this study was to develop a numerical method to predict concrete crack width for corrosion-affected concrete structures. A cohesive crack model for concrete is implemented in the numerical formulation to simulate crack initiation and propagation in concrete. Choices for evaluating the parameters of cohesive elements are extensively discussed which is a key for developing a plausible model employing cohesive elements. The surface crack width is obtained as a function of service time. Accurate prediction of crack width can allow timely maintenance which prolongs the service life of the reinforced concrete structures.

© 2017 Elsevier Ltd. All rights reserved.

## 1. Introduction

Reinforced concrete (RC) structures have been the most common type of structures used in the civil engineering construction since middle nineteenth century. RC structures have been widely used for building, bridges, retaining walls, tunnels, and indeed any physical infrastructure built on and under the ground. Since 1970s, it has become an accepted knowledge that the concrete cover has its limitation on protecting the reinforcing steel from corrosion. As a result, a series of research has been initiated on improving the understanding of the corrosion of steel in concrete [1], such as the Concrete in the Oceans research programme in the UK in the 1970s. Furthermore, it appears to be inevitable that RC structures will suffer from reinforcement corrosion in chloride (Cl<sup>-</sup>) and carbon dioxide (CO<sub>2</sub>) laden environment. Practical experience and experimental observations [2–5] suggest that corrosion affected RC structures deteriorate faster in terms of serviceability (e.g., cracking or deflection) than safety (e.g., strength). Therefore, there is a well justified need for a thorough investigation of the cracking process and crack width of concrete, not least bearing in

mind that crack width is one of the most important practical parameters for the design and assessment of RC structures.

To model cracking of concrete, some researchers have resorted to analytical approach, mainly due to the accuracy of the solution and the convenience of its practical application [6–8]. For example, Li and Yang [7] developed an analytical model for concrete crack width caused by reinforcement corrosion and applied load, by introducing a stiffness reduction factor to account for the post-cracking quasi-brittle behaviour of concrete. The stiffness reduction factor then modifies the differential equation for obtaining the cracked stress and strain components. Correlations between material corrosion and the structural effects can then be established, e.g., crack width [7], time to surface cracking [8], etc. However, the application of analytical modelling in crack propagation in concrete is limited to some special cases, e.g., particular boundary conditions, and the assumption that the crack is smeared and uniformly distributed in the damaged solid to satisfy the requirement on continuous displacement. Some studies have employed complex functions to formulate the stress development under arbitrary boundary conditions [9,10]; however, they have been limited to elastic problems only so far.

In light of the limitation of analytical modelling on crack propagation in concrete, numerical modelling has brought considerable advantages. Depending on the specific application and the scale of

\* Corresponding author.

E-mail address: [shangtong.yang@strath.ac.uk](mailto:shangtong.yang@strath.ac.uk) (S.T. Yang).

the problem, different numerical techniques may be used, e.g., finite element method (FEM) [11,12], discrete element method (DEM) [13], boundary element method (BEM) [14,15] and peridynamics [16,17]. Amongst these numerical methods, FEM has received the most research interest in solving corrosion-induced reinforced concrete cracking. Roesler et al. [11] developed a FE model with cohesive crack concept to predict the fracture performance of concrete beams. A number of geometrically similar beams were investigated and the global mechanical behaviour of the cracked beams was obtained. For corrosion induced concrete cracking, Guzmán et al. [18] developed a concrete cover cracking model based on embedded cohesive crack finite element. Time to surface cracking was then able to be predicted. Sánchez et al. [19] proposed a mesoscopic model simulating the mechanical performance of reinforced beams affected by corrosion. Both cross-sectional and out of cross-section mechanisms, affected by corrosion, were coupled for determination of corrosion effects on the concrete structures. Moreover, Bossio et al. [20] considered the effects of corrosion of four reinforcing rebars on the behaviour of a single structural element. According to the research literature, however, there are very few models on numerical modelling of concrete crack width due to internal pressure such as corrosion induced expansion. Crack width is an important parameter regarding the durability of concrete structures while it is still not quite clear how those underlying factors, e.g., corrosion rate, material/mechanical properties of concrete, may quantitatively affect the development of crack width of the concrete. Therefore, it is well justified that a numerical method be developed to predict corrosion induced concrete crack width over service time.

This paper is based upon Yang et al. [21], but the current paper includes additional research in model formulation, i.e., cracking criteria, choice of parameters of cohesive elements and calculation of corrosion-induced displacement, and a parametric study, i.e., effects of numerical parameters on concrete crack width results. This paper attempts to develop a numerical method to predict the cracking and crack width for corrosion affected concrete structures. Cohesive crack model is used and cohesive elements are embedded for simulating the crack propagation. The choices of parameters of cohesive elements have been extensively discussed which is the key for establishing a plausible model with cohesive elements. After formulation of the model, an example is worked out to demonstrate the application of the method and verification by comparing with analytical/experimental results is provided. Parametric study is finally carried out to investigate the effects of some numerical parameters on the concrete crack width. The crack width obtained from this model is the total crack width which can be used to estimate, with reasonable accuracy, the degradation of concrete cover. It can also be regarded as the maximum possible crack width for design or divided by the number of cracks. Further, this numerical model is highly complimentary to most analytical models, since the same hypothesis was assumed.

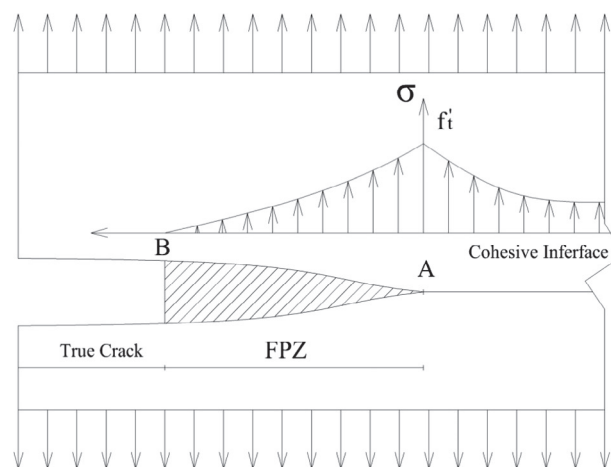
## 2. Constitutive model

The failure of structures is significantly influenced by the properties of the material used. In terms of tensile stress-elongation relationship, most of engineering materials can be classified into brittle, ductile and quasi-brittle [22]. Different materials used will result in different failure mechanisms of structures and hence different material models should be applied correspondingly. For example, Drucker-Prager Model and Von Mises Model are used for ductile materials. For brittle materials, Griffith model based on linear elastic fracture mechanics is usually applied. Cohesive Crack Model, one of few nonlinear fracture mechanics models, is developed and widely used for quasi-brittle materials.

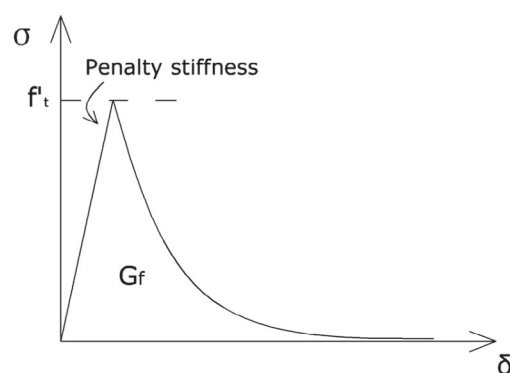
Concrete is considered as a quasi-brittle material, in which the tensile stress gradually decreases after it reaches the tensile strength while the tensile strain/displacement continues to increase. This behaviour of concrete is called strain softening. The concept of strain softening evolves from plasticity where the post-peak decline of the tensile stress is considered as a gradual decrease of the tensile strength, i.e., softening. Since the softening is related to all the strain components, it is normally called strain softening. The reason of strain softening is that there is an inelastic zone developed ahead of the crack tip which is also referred to as fracture process zone (FPZ) as shown in Fig. 1a. When a crack propagates in concrete, the cracked surfaces may be in contact and are tortuous in nature [23], due to various toughening mechanisms such as aggregate bridging, void formation or microcrack shielding [22]. Therefore, the cracked surfaces may still be able to sustain the tensile stress which is characterized by the softening degradation curve.

Cohesive Crack Model (CCM), originally developed by Hillerborg et al. [24], is generally accepted as a realistic simplification for FPZ [25]. CCM assumes that FPZ is long and narrow and is characterized by a stress-displacement curve as typically shown in Fig. 1b. In Fig. 1a, the shadowed zone from point A to B is FPZ and the area beyond Point B is the true crack where the cracked surfaces are completely separated. The CCM is normally incorporated into finite element analysis as an interface when the crack path is known in advance.

Since the FPZ is represented by the cohesive interface and the thickness of the cohesive interface should be very small or zero,



(a) Schematic of mechanism of FPZ



(b) Stress-displacement curve for cohesive material

Fig. 1. Cohesive crack model for the FPZ.

a traction-separation law is introduced to describe its stress-displacement relationship as follows:

$$\sigma = f_{T-S}(\delta) \quad (1)$$

where  $f_{T-S}$  is a nonlinear function, on which a number of researchers have been working to define it. It has been found that with zero thickness, the traction-separation law for the interface provides best estimation for concrete cracking because there is actually no real interface in it. Since  $\delta$  is related to cracking opening displacement  $w$ ,  $f_{T-S}(\delta)$  can also be expressed in terms of  $w$ . As shown in Fig. 1b, there are four parameters to define  $f_{T-S}(\delta)$ : the elastic stiffness (also called penalty stiffness)  $K_p$ , the tensile strength  $f'_t$ , the fracture energy  $G_f$  and the shape of the softening curve.

Since the crack opening  $w$  can be determined via unloading process, the stress-displacement relationship can also be expressed as stress-crack opening relationship. Thus the traction-separation relation for exponential softening curve can be expressed as follows:

$$\sigma = f(w) = f'_t \exp\left(-\frac{f'_t}{G_f} w\right) \quad (2)$$

Once  $f'_t$  and  $G_f$  are known, the constitutive relationship for the cohesive interface can be determined.

As the cracking is assumed to occur at the interface, concrete outside the cracking zone, known as bulk concrete, can be dealt with by linear elastic mechanics. Once a crack occurs, the bulk concrete undergoes unloading. The stress-strain relationship for the bulk concrete is linear as shown below:

$$\sigma' = E\varepsilon' \quad (3)$$

where  $\sigma'$  represents tensile/compressive stress and  $\varepsilon'$  represents the corresponding strain.

Penalty stiffness  $K_p$ : since  $f(w)$  defines only the strain softening after the peak stress  $f'_t$ , the elasticity of the concrete prior to the peak stress needs to be described separately. The initial response of the cohesive interface is assumed to be linear and represented by a constant penalty stiffness ( $K_p$ ) as shown in Fig. 1b. The concept of penalty stiffness comes from the elastic stiffness which is obtained by dividing the elastic modulus of the concrete by its thickness. Since cohesive interface is normally very thin or even of zero thickness, the elastic stiffness of the cohesive interface approaches infinitesimally large. This makes sense as the interface should be stiff enough prior to initiation of crack to hold the two surfaces of the bulk concrete together, leading to the same performance as that of no interface existing. This also meets the condition of CCM which assumes that the energy required to create the new surfaces is vanishingly small compared to that required to separate them [26]. The reason for this condition is that when the elastic stiffness is large, the displacement at tensile strength is small and thus the energy to create the new surfaces is small. However, the elastic stiffness cannot be too large as it will cause convergence problems due to ill-conditioning of the numerical solver of the FE programmes [27]. Therefore, the cohesive stiffness becomes a “penalty” parameter ( $K_p$ ), which controls how easily the cohesive interface deforms elastically. As such this stiffness is large enough to provide the same or close response of intact concrete prior to cracking, but not so large as to cause numerical problems.

Tensile strength  $f'_t$ : The tensile strength  $f'_t$  of concrete material is used as an important index to determine if a cohesive crack is initiated. For Mode I fracture, once the tensile stress at any point of a structure reaches its tensile strength, a crack is initiated and the material of that point starts to degrade. As is known, the tensile strength of concrete can be obtained mainly by three types of tests, which are splitting test, flexural test and direct tensile test. The

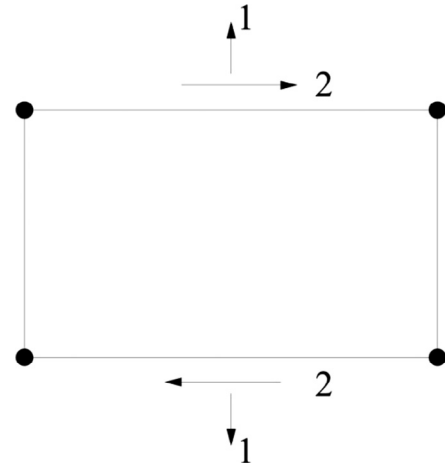


Fig. 2. Local directions for the two-dimensional cohesive element.

strengths measured from these tests vary considerably and  $f'_t$  must be determined via direct tensile test. This is because, in the splitting and flexural tests, the distributed stresses are not pure tension but involving compression. The strength determined from such tests, therefore, is not truly tensile property of concrete.

Fracture energy  $G_f$ : The fracture energy  $G_f$  is the energy absorbed per unit area of crack with the unit of N/mm or N/m. It can be regarded as the external energy supply required to create and fully break a unit surface area of cohesive crack. Therefore,  $G_f$  can be calculated as the area under the softening curve shown in Fig. 1b and expressed as follows

$$G_f = \int_0^{\delta_m} f_{T-S}(\delta) d\delta \quad (4)$$

Since the entire stress-displacement curve  $f_{T-S}(\delta)$  is regarded as a material property,  $G_f$  is also a material parameter which is independent of structural geometry and size.  $G_f$  is used as an energy balance which controls stable crack propagation, that is, a crack will propagate when the strain energy release rate is equal to  $G_f$ .

Shape of softening curve: The cohesive crack initiation is followed by strain softening, which can be represented by a range of forms, e.g., linear, bilinear and non-linear softening. Without knowing the shape of the softening curve, it is difficult to determine the entire stress-displacement curve. Although some researchers have suggested that the exact shape of the softening curve is less important than the values of fracture energy for certain cases [28], the shape of the softening curve is important in predicting the structural response and the local fracture behaviour, i.e. the crack width is particularly sensitive to the shape of the softening curve [22].

### 3. FE simulation

4 nodes cohesive interface element which has two stress components – normal stress in direction 1 and shear stress in direction 2 is used in the simulation (see Fig. 2). There are no other stresses because the thickness in direction 1 is infinitesimally small.

This cohesive interface element will have linear elastic behaviour prior to the peak stress, i.e., tensile strength, followed by the initiation and evolution of damage, i.e., cracking. The elastic constitutive relationship between the nominal stresses and nominal strains is described as follows:

$$\sigma = \begin{Bmatrix} \sigma_1 \\ \sigma_2 \end{Bmatrix} = \begin{bmatrix} E & 0 \\ 0 & G \end{bmatrix} \begin{Bmatrix} \varepsilon_1 \\ \varepsilon_2 \end{Bmatrix} \quad (5)$$

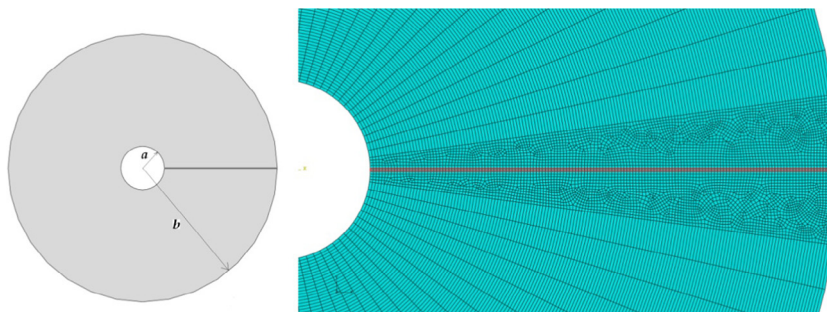


Fig. 3. Geometry of the FE model and the mesh around the cohesive interface.

where  $\sigma_1$  and  $\sigma_2$  are the normal stress in direction 1 and shear stress in direction 2 respectively,  $G$  is the shear modulus in plane state (in 2D), and  $\varepsilon_1$  and  $\varepsilon_2$  are the corresponding strains of  $\sigma_1$  and  $\sigma_2$ .

For concrete with embedded reinforcing steel bar, it is widely accepted to be modelled as a thick-wall cylinder [6,29]. Fig. 3 shows the geometry of the cylinder as well as the placement of cohesive interface. It is assumed that only one crack will initiate and propagate from the inner boundary of the cylinder to the outer boundary. However, this crack represents the total cracks in a way that the total crack width can be divided by the number of the cracks, as widely employed in smeared crack model. For FEA, two elements are employed in this study: 4 nodes cohesive interface element as discussed earlier for the cohesive interface, and 4 nodes bilinear plane strain quadrilateral element for the bulk concrete. Reduced integration is used for the plane strain element because the accuracy of the bulk concrete is not an issue. As a result, the damage evolution of the cohesive element is combined with the elastic deformation of the bulk concrete in the global response.

Additionally, very fine mesh is used in the cohesive interface and its surrounding bulk concrete. The thickness of the cohesive interface is 0.2 mm and the inner radius and outer radius are 6 mm and 37 mm respectively. Since the cohesive interface should only accommodate a single layer of cohesive elements due to traction-separation law, the element size of the cohesive element is chosen as 0.2 mm. The region around the cohesive interface will have stress concentration during the cracking process of the cohesive elements which should have the same element size as the cohesive element. The other area of the bulk concrete is in pure linear elasticity and has no concentration of stress; therefore, much coarser mesh can be applied. It has been tried on this selected mesh size to ensure that the convergence is not the problem due to the mesh size.

The cylinder is subjected to a uniformly distributed pressure at the inner boundary, i.e., the corrosion induced pressure and applied load induced pressure. For brittle and ductile materials, pressure/force can be directly applied to the boundary. However, for strain softening materials, only displacement can be used as boundary condition. This is because, the far field force/stress, does not monotonically increase; instead, it will drop after initial increase. However, the displacement always increases and this is why displacement should be applied as boundary condition for strain-softening materials. In this model, the expansion cannot be just uniformly distributed due to the introduction of the cohesive interface. The reason is that if the radial displacement is applied uniformly in a polar coordinate system, there will be a component in the normal direction (direction 1 in Fig. 2) of the 1st cohesive element at the inner boundary because of its finite geometric thickness, which is illustrated in Fig. 4. The component can only be waived if the cohesive elements are geometrically modelled as zero thickness, which will lead to the expansion in

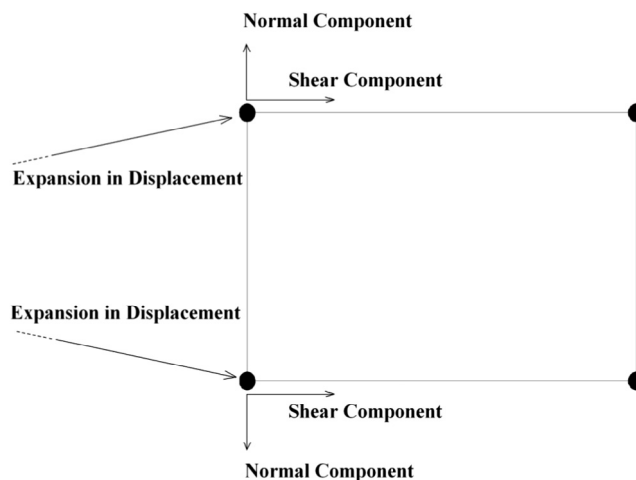


Fig. 4. Stresses of the 1st cohesive element under uniform load distribution.

Fig. 4 in horizontal direction. Such a displacement component results in dramatically large stress since the stiffness of the cohesive elements are much larger than the surrounding bulk concrete.

Due to the fact that the displacement (normal component) cannot be directly applied to the 1st cohesive element, the displacement is applied in two coordinate systems in this study. The displacement applied to the cohesive element is defined in direction of x-axis in rectangular coordinate system, and the displacement applied to the other part of the inner boundary is defined in radial direction in cylindrical coordinate system. With this arrangement, the geometric thickness of the cohesive element needs to be very small. This arrangement eliminates the normal component of the displacement on the 1st cohesive element and approximately reserves the shear component of the displacement. Since the thickness of the cohesive element is extremely small, the shear component of the uniformly distributed displacement can be considered the same as the distributed displacement itself. Under this arrangement, the traction of the cohesive element comes from the deformation of the whole cylinder and there is no artificial displacement added to the normal direction of the cohesive element.

The inner displacement boundary condition of the concrete is caused by reinforcement corrosion which can be calculated by analytical means. According to Li and Yang [7] formulated the corrosion-induced reinforcement expansion volume and the displacement at the inner boundary of the concrete. Details about the analytical formulation can be referred to Li and Yang [7] while the corrosion-induced displacement of expansion  $d_c(t)$  is listed as follows:

$$d_c(t) = \frac{W_{rust}(t)}{\pi D} \left( \frac{1}{\rho_{rust}} - \frac{\alpha_{rust}}{\rho_{st}} \right) - d_0 \quad (6)$$

where  $D$  is diameter of the reinforcing rebar,  $d_0$  is the thickness of the interfacial porous band between concrete and reinforcement,  $\alpha_{rust}$  is the molecular weight of steel divided by the molecular weight of corrosion products. It varies from 0.523 to 0.622 according to different types of corrosion products [30].  $\rho_{rust}$  and  $\rho_{st}$  are the densities of corrosion products and the original steel, respectively.  $W_{rust}(t)$  is related to the corrosion rate of the steel rebar and can be expressed as follows [7]:

$$W_{rust}(t) = \sqrt{2 \int_0^t 0.105(1/\alpha_{rust})\pi D i_{corr}(t) dt} \quad (7)$$

where  $i_{corr}$  is the corrosion current density in  $\mu A/cm^2$ , which is widely used as a measure of corrosion rate.

By using Eqs. (6) and (7), the time-dependent displacement of the inner boundary of the concrete cylinder can be obtained for FE analysis, as illustrated in Fig. 5.

Crack initiation marks the beginning of degradation or damage of concrete at a point. Crack is assumed to initiate when the maximum nominal tensile stress reaches the tensile strength of the concrete for the Mode I fracture – opening mode, expressed as follows

$$\langle \sigma_1 \rangle = f'_t \quad (8)$$

$$\text{where } \langle \sigma_1 \rangle = \begin{cases} \sigma_1 & \text{for } \sigma_1 > 0 \\ 0 & \text{for } \sigma_1 < 0 \end{cases}$$

The operation  $\langle \sigma_1 \rangle$  is to ensure that a crack will not initiate under compression.

After cracking is initiated, the cohesive element is damaged and the normal stress of this element softens in a manner as defined (e.g., Fig. 1b). The failure of the element is governed by the softening curve. To calculate the residual stress after its peak/cracking stress, a damage parameter  $D$  is introduced into the stress calculation as follows:

$$\sigma = (1 - D)\sigma_u \quad (9a)$$

$$\sigma_u = K_p \delta \quad (9b)$$

where  $\sigma_u$  is the undamaged stress as shown in Fig. 6.

To prevent mesh sensitivity in FE analysis, the damage evolution has to be based on displacement or energy rather than strain. This means the crack opening is not dependent on the strain of the element but the opening distance of the element. Therefore, as the distance between the nodes is used as a crack measure rather than a change in strain (which depends on the element length) the mesh dependency is significantly reduced.

To calculate the residual stress after its peak/cracking stress, a damage parameter  $D$  is defined as follows

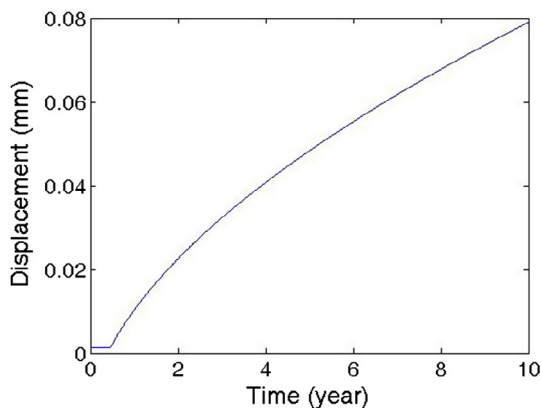


Fig. 5. Internal expansion (displacement) as function of service time.

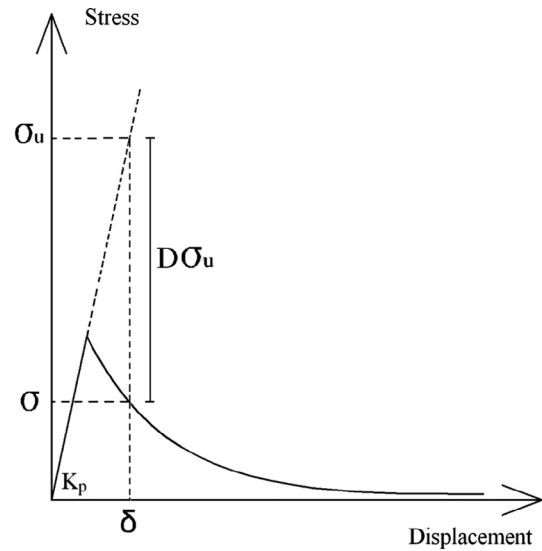


Fig. 6. Determination of residual stress in terms of the damage parameter  $D$ .

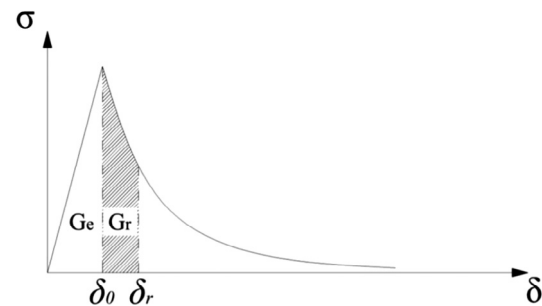


Fig. 7. Illustration of various energy release rates.

$$D = \frac{G_r}{G_f - G_e} = \frac{\int_{\delta_0}^{\delta_r} f_{T-S}(\delta) d\delta}{G_f - \frac{f_t \delta_0}{2}} \quad (10)$$

where  $G_r$  is the energy release rate after peak stress,  $G_e$  is the elastic energy release rate prior to peak stress. These energy parameters are illustrated in Fig. 7.

Convergence is usually a problem in the execution of FE programmes for materials exhibiting softening behaviour for implicit scheme as in most FE programmes. Also, when a material is damaged, e.g., concrete is cracked, sudden dissipation of energy will make the computation more dynamical while the quasi-static analysis is expected. An artificial viscosity is therefore used to overcome the convergence difficulties by making the stiffness matrix of the material positive. This viscosity regularizes the traction-separation law by modifying the stiffness reduction variable  $D$  as follows

$$\dot{D}_v = \frac{D - D_v}{\mu} \quad (11)$$

where  $\mu$  is the viscosity parameter which can be specified in the property of cohesive element and  $D_v$  is the viscous stiffness degradation variable. Once  $\mu$  and  $D$  are known,  $D_v$  can be determined. A small viscosity value  $\mu$  helps improve the rate of convergence without compromising results.

#### 4. Worked example

As a demonstration of the application of the developed numerical method and techniques in FEA, the example used in Li [3] is

taken for numerical solutions. The loading is applied to the concrete in the form of displacement rather than pressure, due to the strain softening behaviour as explained previously. Fig. 5 shows the displacement applied to the concrete as a function of service time which can be calculated analytically using classic mechanics. In this example, the stress-displacement relationship is taken from the direct tensile test, as shown in Fig. 7.

The values of the basic variables used in the numerical solution are listed in Table 1. To calculate the effective modulus of elasticity, the creep coefficient is taken as 2.0. Since the cohesive element size is of 0.0002 m and the theoretical thickness of the cohesive element is 1, the elastic stiffness of the cohesive interface is 35,250 GPa ( $5000E_{cf}$ ). However, due to the value is too large, the penalty stiffness is taken as 14,100 GPa ( $2000E_{cf}$ ). The time-dependant internal displacement, i.e., Fig. 5, is applied to the concrete cylinder as the boundary displacement condition. The constitutive stress-displacement relation is obtained from the direct tensile test on concrete. The stress-inelastic effective displacement curve can be plotted in Fig. 8.

The crack finally approaches the outer boundary of the cylinder (surface). Since the theoretical thickness of the cohesive element is set to be 1.0, the strain of the cohesive element is equal to its displacement. Upon removing the elastic displacement from the total displacement of the last cohesive element at the outer boundary of the cylinder, the surface crack width can be expressed in a function of time, shown in Fig. 9.

In Fig. 9, it can be seen that the surface crack width increases with time. The abrupt increase in the crack width corresponds to rapid decrease of tensile stress, or sudden energy release, in the element as shown in Fig. 8. After about 4 years, the increase of the crack width is steady and seems to approach certain value after about 7 years. This might be due to a combined effect of the steady decrease of the tensile stress (long tail of the stress-displacement curve in Fig. 8) and the nonlinear development of displacement applied at the inner boundary (i.e., Fig. 5). At 10 years, the crack width reaches about 0.23 mm.

To verify the proposed numerical method, the results are compared with those from the recently developed analytical model [7]. By using the same inputs, which are mainly from Li [31] and Liu and Weyers [30], the resulted crack width from both methods can be compared as a function of service time, as shown in Fig. 10. It can be seen that the numerical results are in good agreement with the analytical results. The crack width derived from the analytical model has been verified against the experiment data (i.e., Fig. 9 in [7]). Hence, in this paper, the analytical results on crack width are used as the reference for validating the numerical model. Further, the results of the numerical model are compared with experimental data for validation. Table 2 shows the comparison of time-to-surface cracking from a number of analytical, numerical and experimental models. Details of these literatures are not repeated here but can be easily obtained from various sources. By using the same values of variables in the original literature, the surface cracking time can be obtained and presented in Table 2.

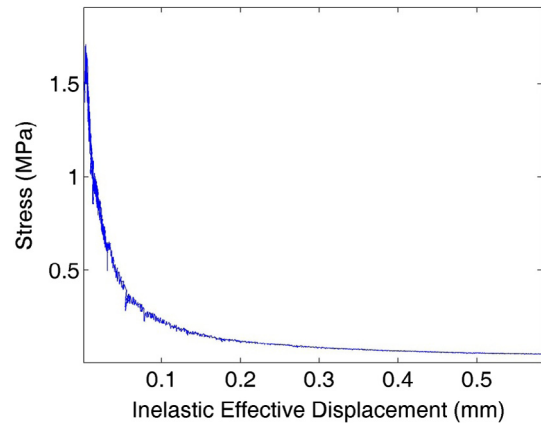


Fig. 8. Constitutive relation inputs for CCM used in the example.

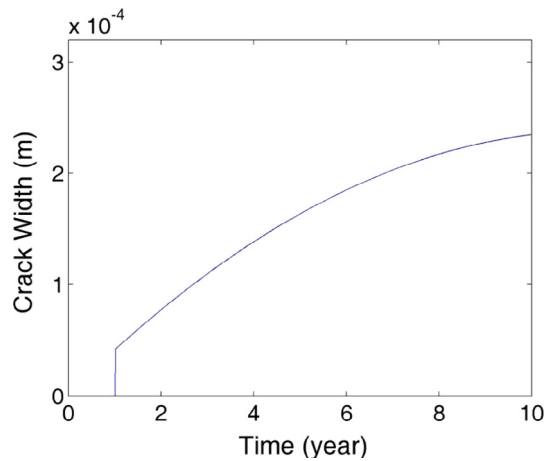


Fig. 9. Crack width as a function of time.

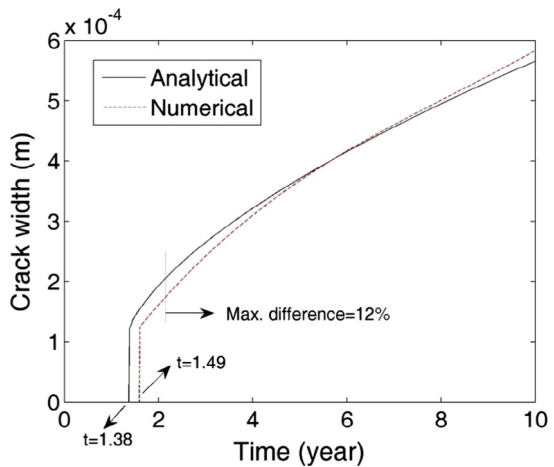


Fig. 10. Crack widths as a function of time by both methods.

Table 1 Values of basic variables used in the example.

Description	Symbol	Values	Sources
Inner radius	$a$	6 mm	Li [3]
Outer radius	$b$	37 mm	Li [3]
Effective modulus of Elasticity	$E_{ef}$	7.05 GPa	Experiment
Poisson's ratio	$\nu_c$	0.18	Li [3]
Tensile strength	$f'_t$	1.7 MPa	Experiment
Fracture energy	$G_f$	65 N/m	Experiment

Table 2 Comparison of time-to-surface cracking.

Model	Time-to-surface cracking (in years)
Analytical (Li et al., 2006)	3.49
Analytical (Pantazopoulou and Papoulia, 2001)	3.50
Experimental (Liu and Weyers, 1998)	3.54
Numerical (current model)	3.67

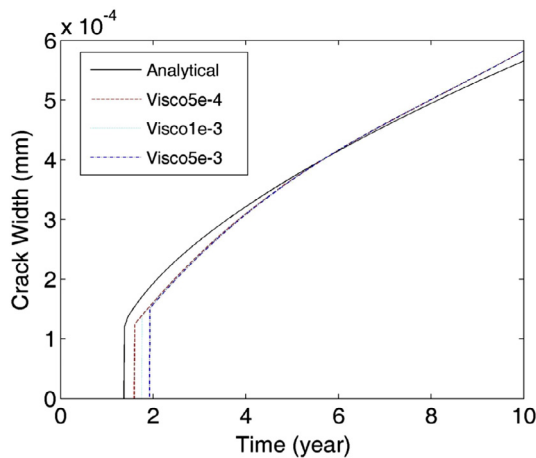


Fig. 11. Effect of viscous regularization on the predicted concrete crack width.

As discussed, the results of materials exhibiting softening behaviour and degradation of stiffness will normally have severe convergence problems. A common numerical technique to solve the convergence difficulty is to employ a small viscosity value to regularize the constitutive equations, as presented in Eq. (9). Fig. 11 shows the effect of the viscous regularization on the predicted concrete crack width with three viscosity values used. Visco5e-4, Visco1e-3 and Visco5e-3 represent viscosity values of 5e-4, 1e-3 and 5e-3 respectively. The analytical result [7] is also plotted in Fig. 11 for comparison. Smaller viscosity values, i.e. 1e-4, have been used but no converged results have been obtained. It can be seen from Fig. 11 that the viscosity value of 5e-4 matches best with the analytical results. Higher viscosity values provide better convergence, i.e., easier to converge and less increments required, but also affect the results more than the lower values of viscosity. Therefore, the viscosity coefficient should be kept as small as it can make the analysis be converged. In this example, the appropriate value of viscosity coefficient is considered as 5e-4.

Penalty stiffness is the cohesive stiffness as shown in Fig. 1b which controls how easily the cohesive interface deforms elastically. To investigate its effect on the results of concrete crack width, three values of penalty stiffness are employed and the results are shown in Fig. 12. Penalty1, Penalty2 and Penalty3 represent the values of penalty stiffness of 14,100 GPa, 7050 GPa and 3525 respectively. 14,100 GPa was used in the worked example. It can be seen that smaller penalty stiffness makes the surface

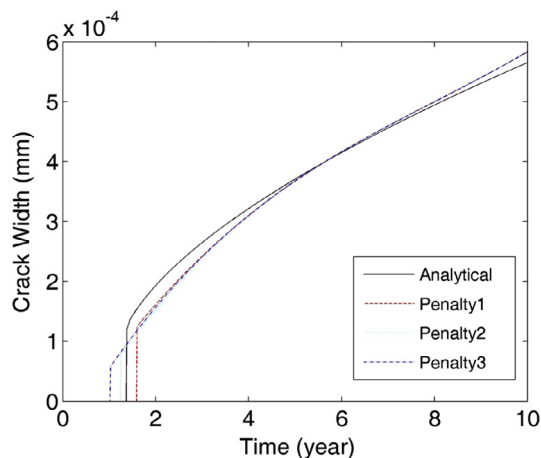


Fig. 12. Effect of penalty stiffness on predicted concrete crack width.

cracking time earlier. There might be confusion herein that the penalty stiffness controls the elasticity of the cohesive elements but it does affect the concrete crack width which is mainly controlled by the inelastic behaviour of the cohesive elements. This can be explained by using Fig. 6 that the calculation of the residual tensile stress is dependent on the undamaged stress  $\sigma_u$  which is determined by the penalty stiffness. Therefore the energy required to break a unit cohesive surface (fracture energy) is influenced by the penalty stiffness. It thus explains why the early stage of cracking, i.e., surface cracking initiation, is sensitive to the change of penalty stiffness. However, the long-term development of crack width seems not affected by the penalty stiffness. The reason for that could be the long-term development of crack width is considerably influenced by the tail of the stress-displacement curve as shown in Fig. 6. The tail of the curve is, however, negligibly affected by the penalty stiffness.

## 5. Conclusions

A numerical method to predict the crack width induced by reinforcement corrosion has been developed based on fracture mechanics and using finite element method. The concept of cohesive process zone has been employed to model the cracking behaviour of concrete whose constitutive relationship is characterized by a traction-separation law. A worked example has been presented to first demonstrate the application of the derived method and then compare with the results from an analytical method as a means of verification. It has been found that the numerical results are in good agreement with the analytical results, with an average difference of 4% within 10 years. It can be concluded that the numerical method presented in the paper can predict the concrete crack width induced by reinforcement corrosion with reasonable accuracy.

## Acknowledgement

The authors wish to acknowledge the support of the European Commission via the Marie Curie IRSES project GREAT - Geotechnical and geological Responses to climate change: Exchanging Approaches and Technologies on a world-wide scale (FP7-PEOPLE-2013-IRSES-612665). Financial support from Scottish Funding Council GRPE for early career researcher exchanges is also gratefully acknowledged.

## References

- [1] Wilkins NJM, Lawrence PF. Concrete in the oceans: fundamental mechanics of corrosion of steel reinforcements in concrete immersed in sea water. UK: Slough; 1980.
- [2] Andrade C, Molina FJ, Alonso C. Cover cracking as a function of rebar corrosion: part 1 - experiment test. Mater Struct 1993;26:453-4.
- [3] Li CQ. Life-cycle modelling of corrosion-affected concrete structures: propagation. ASCE J Struct Eng 2003;129(6):753-61.
- [4] Li CQ. Time dependent reliability analysis of the serviceability of corrosion affected concrete structures. Int J Mater Struct Reliab 2005;3(2):105-16.
- [5] Otsuki N, Miyazato S, Diola NB, et al. Influences of bending crack and water-cement ratio on chloride-induced corrosion of main reinforcing bars and stirrups. ACI Mater J 2000;97(4):454-65.
- [6] Pantazopoulou SJ, Papoulia KD. Modeling cover cracking due to reinforcement corrosion in RC structures. J Eng Mech, ASCE 2001;127(4):342-51.
- [7] Li CQ, Yang ST. Prediction of concrete crack width under combined reinforcement corrosion and applied load. J Eng Mech, ASCE 2011;137(11):722-31.
- [8] Bhargava K, Ghosh AK, Mori Y. Model for cover cracking due to rebar corrosion in RC structures. Eng Struct 2006;28(8):1093-109. 7//.
- [9] Yang ST, Li KF, Li CQ. Analytical model for non-uniform corrosion-induced concrete cracking. Mag Concr Res 2017 [in press].
- [10] Xia N, Ren Q, Liang RY, Payer J. Nonuniform corrosion-induced stresses in steel-reinforced concrete. J Eng Mech, ASCE 2012;138.
- [11] Roesler J, Paulino GH, Park K, et al. Concrete fracture prediction using bilinear softening. Cem Concr Compos 2007;29:300-12.

- [12] Hanson JH, Ingraffea AR. Using numerical simulations to compare the fracture toughness values for concrete from the size-effect, two-parameter and fictitious crack models. *Eng Fract Mech* 2003;70:1015–27.
- [13] Beckmann B, Schicktan K, Reischl D. DEM simulation of concrete fracture and crack evolution. *Struct Concr* 2012;13(4):213–20.
- [14] Aliabadi MH, Saleh AL. Fracture mechanics analysis of cracking in plain and reinforced concrete using the boundary element method. *Eng Fract Mech* 2002;69(2):267–80.
- [15] Chahrour AH, Ohtsu M. BEM analysis of crack propagation in concrete based on fracture mechanics. In: Kobayashi S, Nishimura N, editors. *Boundary element methods: fundamentals and applications*. Berlin, Heidelberg: Springer; 1992. p. 59–66.
- [16] Huang D, Lu G, Liu Y. Nonlocal peridynamic modeling and simulation on crack propagation in concrete structures. *Math Probl Eng* 2015;2015:11.
- [17] Gerstle W, Sau N, Silling S. Peridynamic modeling of concrete structures. *Nucl Eng Des* 2007;237(12–13):1250–8. 7//.
- [18] Guzmán S, Gálvez JC, Sancho JM. Modelling of corrosion-induced cover cracking in reinforced concrete by an embedded cohesive crack finite element. *Eng Fract Mech* 2012;93:92–107. 10//.
- [19] Sánchez PJ, Huespe AE, Oliver J, et al. Mesoscopic model to simulate the mechanical behavior of reinforced concrete members affected by corrosion. *Int J Solids Struct* 2010;47(5):559–70. 3/1/.
- [20] Bossio A, Monetta T, Bellucci F, et al. Modeling of concrete cracking due to corrosion process of reinforcement bars. *Cem Concr Res* 2015;71:78–92. 5//.
- [21] Yang ST, Li KF, Li CQ. Numerical model for concrete crack width caused by reinforcement corrosion and applied load. In: 15th International conference on civil, structural and environmental engineering computing, Prague, Czech Republic.
- [22] Shah SP, Swartz SE, Ouyang C. *Fracture mechanics of concrete: applications of fracture mechanics to concrete, rock, and other quasi-brittle materials*. New York: John Wiley & Sons Inc; 1995. p. 552.
- [23] Mindess S, Diamond S. *The cracking and fracture of mortar*. *Mater Struct* 1982;15(86):107–13.
- [24] Hillerborg A, Modeer M, Petersson PE. Analysis of crack formation and crack growth in concrete by means of fracture mechanics and finite elements. *Cem Concr Res* 1976;6(6):773–81.
- [25] Elices M, Rocco C, Rosello C. Cohesive crack modeling of a simple concrete: experimental and numerical results. *Eng Fract Mech* 2009;76(10):1398–410.
- [26] Bažant ZP, Planas J. *Fracture and size effect in concrete and other quasibrittle materials*. Boca Raton (Florida): CRC Press; 1998.
- [27] A. C. 446.3R. *Finite element analysis of fracture in concrete structures*. Farmington Hills, Mich; 1997.
- [28] Elices M, Guinea GV, Gomez J, et al. The cohesive zone model: advantages, limitations and challenge. *Eng Fract Mech* 2002;69:137–63.
- [29] Tepfers R. Cracking of concrete cover along anchored deformed reinforcing bars. *Mag Concr Res* 1979;31(106):3–12.
- [30] Liu Y, Weyers RE. Modelling the time-to-corrosion cracking in chloride contaminated reinforced concrete structures. *ACI Mater J* 1998;95(6):675–81.
- [31] Li CQ. Life cycle modelling of corrosion affected concrete structures – propagation. *J Struct Eng, ASCE* 2003;129(6):753–61.